







Simultaneous characterization of cross- and in-plane thermal transport in insulator patterned by directionally aligned nano-channels

Cite as: AIP Advances **10**, 015304 (2020); <https://doi.org/10.1063/1.5125415>

Submitted: 24 October 2019 . Accepted: 17 December 2019 . Published Online: 06 January 2020

Vinay S. Chauhan , Azat Abdullaev , Zhandos Utegulov , Jacques O'Connell , Vladimir Skuratov , and Marat Khafizov 



View Online



Export Citation



CrossMark

ARTICLES YOU MAY BE INTERESTED IN

[Thermal transport across nanoscale damage profile in sapphire irradiated by swift heavy ions](#)

Journal of Applied Physics **127**, 035108 (2020); <https://doi.org/10.1063/1.5126413>

[Analysis of heat flow in layered structures for time-domain thermoreflectance](#)

Review of Scientific Instruments **75**, 5119 (2004); <https://doi.org/10.1063/1.1819431>

[Tutorial: Time-domain thermoreflectance \(TDTR\) for thermal property characterization of bulk and thin film materials](#)

Journal of Applied Physics **124**, 161103 (2018); <https://doi.org/10.1063/1.5046944>



NEW!

Sign up for topic alerts
New articles delivered to your inbox



Simultaneous characterization of cross- and in-plane thermal transport in insulator patterned by directionally aligned nano-channels

Cite as: AIP Advances 10, 015304 (2020); doi: 10.1063/1.5125415

Submitted: 24 October 2019 • Accepted: 17 December 2019 •

Published Online: 6 January 2020



View Online



Export Citation



CrossMark

Vinay S. Chauhan,¹  Azat Abdullaev,²  Zhandos Utegulov,²  Jacques O'Connell,³ 
Vladimir Skuratov,^{4,5,6}  and Marat Khafizov^{1,a)} 

AFFILIATIONS

¹Department of Mechanical and Aerospace Engineering, The Ohio State University, Columbus, Ohio 43210, USA

²Department of Physics, School of Sciences and Humanities, Nazarbayev University, Nur-Sultan 010000, Kazakhstan

³Centre for HRTEM, Nelson Mandela University, Port Elizabeth 6019, South Africa

⁴Flerov Laboratory of Nuclear Reactions, Joint Institute for Nuclear Research, Dubna 141980, Russia

⁵Division of Nuclear Physics and Technologies, National Research Nuclear University MEPhI, Moscow 115409, Russia

⁶Faculty of Natural and Engineering Science, Dubna State University, Dubna, Moscow Region, 141982, Russia

^{a)} Author to whom correspondence should be addressed: khafizov.1@osu.edu

ABSTRACT

Anisotropic thermal transport behavior was investigated in a single crystal sapphire patterned by vertically aligned few-nanometer diameter and several micrometer long cylindrical ion tracks. These ion tracks were introduced by exposing the sapphire to energetic ions of xenon accelerated to 167 MeV with fluences ranging from 10^{12} to 10^{14} ions/cm². It was found that, in the low ion-track density regime, cross-plane thermal conductivity is larger, whereas in the high track density regime, the trend reverses and in-plane conductivity becomes larger. The crossover between these regimes is attributed to the interplay between phonon scattering with ion track boundaries and phonon confinement effects. In the low track density regime, the material is described by bulk phonon dispersion and anisotropy in thermal transport is attributed to the aligned nature of tracks that effectively reduce the mean free path of phonons traveling in the in-plane direction more than in the cross-plane direction. In the high-density regime, larger conductivity reduction in the cross-plane direction is consistent with previous observations, where the anisotropic reduction in thermal conductivity is owed to the anisotropic reduction of acoustic velocity caused by phonon confinement. Our results are further supported by an analytical model describing phonon mediated thermal transport.

© 2020 Author(s). All article content, except where otherwise noted, is licensed under a Creative Commons Attribution (CC BY) license (<http://creativecommons.org/licenses/by/4.0/>). <https://doi.org/10.1063/1.5125415>

Tailoring and understanding heat transport characteristics of materials at the nanoscale has drawn significant attention due to a necessity to address thermal management needs in thermoelectrics, electronics, and advanced energy conversion systems.^{1–4} Device performance of certain applications can benefit from heat flow in preferential directions owing to intrinsic or induced thermal transport anisotropy. Recently, motivated by thermal management applications, anisotropic thermal conductivity has been investigated in graphene, pyrolytic carbon, hexagonal boron nitride, and similar two-dimensional materials and thin silicon films.^{5–12}

Multiple micro- and nanofabrication techniques of composites consisting of aligned carbon nanotubes, nanowires, thin films, or porosity have been exploited to make materials conduct heat preferentially in one direction.^{13–15} However, the impact of interfaces on thermal transport and their role in anisotropic conductivity remains an open question. Also, they offer an avenue for further exploring nanoscale thermal transport phenomena. Here, we explore an alternative method for inducing anisotropic thermal conductivity, which introduces an aligned array of nanochannels in insulating and semiconductor materials by swift heavy ion (SHI) irradiation.

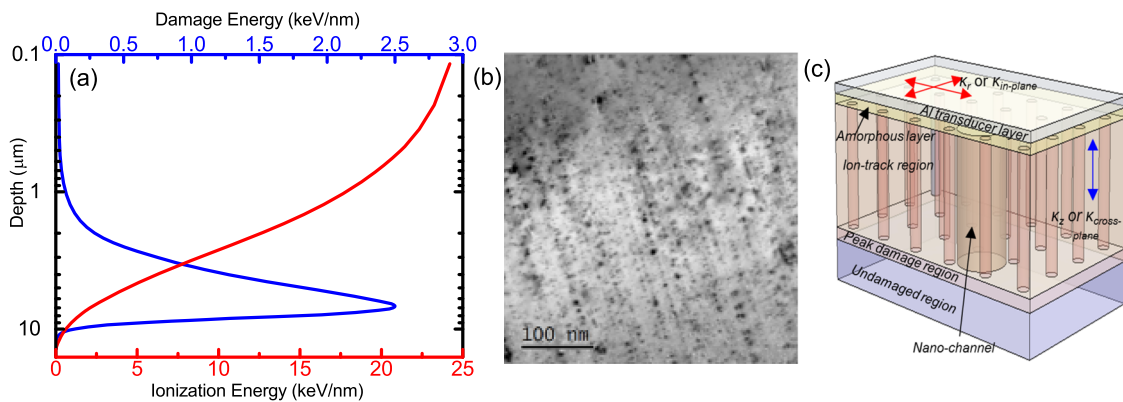


FIG. 1. (a) Variation of the damage profile caused by electronic (red) and nuclear (blue) stopping. (b) Bright field TEM micrograph of $2 \times 10^{12} \text{ cm}^{-2}$ irradiated Al_2O_3 viewed in cross section. (c) Schematics depicting different regions of the patterned Al_2O_3 and direction along which conductivity was measured. Lighter contrast cylinders are ion tracks, while the darker cylinder confined between ion tracks represents a nanochannel.

Latent ion tracks induced by the SHI offer an attractive method for patterning an aligned array of nanochannels to modify material properties.^{16,17} Utilization of these nanochannel arrays has been explored to tailor electronic, photonic, and ionic properties of metal oxides.^{18,19} We are extending the application of these nanochannels to tailor the thermal transport properties. In this letter, we demonstrate the use of SHI irradiation to modify the anisotropy in thermal conductivity of sapphire. Sapphire is particularly chosen as a model system here owing to the fact that its response to the SHI is well documented and there is a well-established procedure for introduction of ion tracks.^{16,20,21}

Pristine sapphire's anisotropy in thermal transport (~ 1.08) is defined as the ratio of in-plane (κ_x) to cross-plane (κ_z) thermal conductivity and stems from its trigonal crystalline structure.²² The slight anisotropic thermal conductivity is attributed to different sound velocities along a - and c -directions of its crystalline lattice, and phonon anharmonicity is usually neglected for practical applications.^{22,23}

Currently, the formation of ion tracks has been demonstrated in a range of materials, including intrinsically cubic materials.^{18,19} Near the surface, energy transfer by projectile ions to the target atoms is dominated by inelastic electronic stopping that thermally excites electrons along the ion path. Under appropriate conditions, governed by electron-phonon coupling and lattice thermal conductivity, this leads to an intense localized thermal spike which induces melting of a region confined to a few nanometer diameter cylindrical core (ion track) and negligible displacement damage outside of the core region.¹⁶ These nanostructured channels whose boundaries are defined by ion-tracks present an attractive system for tailoring anisotropic heat transfer characteristics and understanding nanoscale thermal transport. We analyze this phenomenon by simultaneous measurement of cross- and in-plane thermal conductivities.^{24–27} The interplay between specular and diffuse reflections of phonons from ion track boundaries, phonon confinement effects, and phonon mean free path (MFP) changes are expected to be contributing factors in determining anisotropic thermal transport in these structures.^{28,29} It should be emphasized that discussion

presented here is expected to be applicable even to intrinsically isotropic materials.

Single c -cut crystals were irradiated at 300 K by 167 MeV Xe ions with fluences ranging from 10^{12} to 10^{14} cm^{-2} at the IC-100 FLNR JINR cyclotron in Dubna, Russia. The SRIM-2013 code was used to estimate the damage profile of the impacted layer using the full cascade mode.³⁰ The threshold displacement energies of Al and O were set as 17 and 76 eV, respectively.³¹ Figure 1(a) shows electronic and nuclear stopping profiles and is used to estimate the depth of different regions of the ion impacted layer. The length of ion tracks is estimated to be $7.6 \pm 0.1 \mu\text{m}$ using a track formation threshold of 9.8–10.5 keV/nm.^{16,32,33} A bright field transmission electron microscopy (TEM) image of the $2 \times 10^{12} \text{ cm}^{-2}$ sample is shown in Fig. 1(b) and confirms the presence of ion-tracks, represented by discontinuous lines of dark contrast extending from the irradiated surface into the crystal. The morphology of the ion track in Al_2O_3 is different from that of most other materials, where ion tracks have been observed and represented by amorphous regions. In our subsequent analysis, to maintain the discussion applicable across a broad range of ion track morphologies, we approximate this linearly aligned array of pores observed in TEM [Fig. 1(b)] by cylindrical inclusions, as shown in Fig. 1(c). In this approximation, these cylinders have different elastic and thermal properties, as they have effectively lower density caused by porosity (in Al_2O_3), amorphous structure, or extensive disorder.³⁴ From the thermal transport perspective, the cylinder surface is expected to scatter phonons in a similar manner that surface or interface boundaries scatter phonons in thin films, nanowires, and superlattices.^{4,11,15,24}

At low ion fluence (below $4 \times 10^{12} \text{ cm}^{-2}$), ions are likely to propagate through the unperturbed region and isolated tracks are formed whose average effective diameter has been reported to be 1.8 nm.^{16,32} As ion fluence is increased, incident ions are likely to propagate through regions that have been already impacted. In this overlapping track regime, the pre-existing track is recovered and a new larger diameter track is formed with some disorder around the track.³² The minimum distance between two tracks in Al_2O_3 has been reported to be $\sim 5.4 \text{ nm}$, corresponding to a saturation

fluence of $4.3 \times 10^{12} \text{ cm}^{-2}$, which can be considered the threshold fluence limit for the overlapping track regime.³² Further increase in ion fluence leads to the formation of an amorphous layer at the sample surface caused by incomplete recovery of pre-existing ion tracks in the overlapping regime. Figure 1(c) shows a schematic of the patterned sapphire structure as used for thermal transport analysis, which captures the amorphous layer (few tens of nanometer), ion track region represented by cylindrical inclusions ($8 \mu\text{m}$), peak damage layer ($2 \mu\text{m}$), and undamaged bulk region. The intermediate region where ion tracks end, but nuclear stopping is not sufficiently strong, is considered a part of the peak damage region. It is not separately accounted for in this work to simplify the thermal transport analysis.

Modulated thermoreflectance (MTR) technique was used to measure thermal conductivity of pristine and irradiated sapphire.^{35–37} The details of the experimental setup and associated analysis to extract conductivities and interface conductance have been reported in previous publications.^{37–41} Prior to MTR characterization, a 106-nm thick Al metal transducer layer was deposited on the sample surface [Fig. 1(b)] whose thickness was measured using picosecond acoustics. Thermal conductivity $\kappa_{Al} = 110 \text{ W/m K}$ of the transducer layer was measured using a reference sample.³⁷

Amplitude and phase of spatially resolved thermal wave profiles were recorded and analyzed over the 1–100 kHz modulation frequency range. This frequency range was found to be optimal for measuring both in-plane and cross-plane conductivities of patterned Al_2O_3 . For the extraction of thermal conductivity, the phase profiles were analyzed using the frequency domain solution of the heat diffusion equation with a multilayer representation of the damaged region while taking into consideration that the ion track region [Fig. 1(c)] is expected to exhibit anisotropic thermal transport properties. The solution is considered in cylindrical coordinates due to axial symmetry imposed by the orientation of the tracks and c-cut of the crystal.^{37–41}

Anisotropic heat conduction is described by the heat diffusion equation considering different in-plane κ_r and cross-plane κ_z thermal conductivities,

$$\rho c \frac{\partial T}{\partial t} = \kappa_z \nabla_z^2 T + \kappa_r \nabla_r^2 T + Q e^{i2\pi f t}, \quad (1)$$

where T is the temperature, r and z are spatial coordinates, t is the time, f is the modulation frequency, ρ is the density, c is the specific heat of the material, and Q is the power of the heat source. For the isotropic case, conductivities in Eq. (1) are assumed to be the same with $\kappa_r = \kappa_z = \kappa_0$.

For the irradiated samples, the nonhomogeneous damage profile was approximated by a few layers with uniform thermal properties, as shown in Fig. 1(c). Samples with fluence $< 5 \times 10^{13} \text{ cm}^{-2}$ were analyzed using a three-layer model consisting of an Al transducer, the ion-track region, and the undamaged region.⁴¹ In this analysis, cross-plane conductivity (κ_z) and in-plane conductivity (κ_r) of the ion-track layer and interface thermal resistance (R_{th}) between the transducer and the sapphire were used as fitting parameters. Other required parameters were assumed to be known and obtained from the literature. In the high fluence regime ($\geq 5 \times 10^{13} \text{ cm}^{-2}$), an additional thin amorphous layer on top of the damaged layer was included. The conductivity of the amorphous layer was estimated as $1.57 \text{ W/m}\cdot\text{K}$ using a minimum thermal conductivity expression

from Ref. 42 based on $c = 780 \text{ J/kg K}$ and $\rho = 2900 \text{ kg/m}^3$.⁴³ In order to reduce the number of fitting parameters, in the case of higher fluence samples, the thickness of the amorphous layer was determined using either TEM or time domain thermoreflectance (TDTR) which provides greater sensitivity to a thin amorphous layer.⁴⁴

To demonstrate the anisotropy in the patterned structure, we summarize the results of the analysis by presenting slopes of the measured thermal wave profiles.⁴¹ The linear sections of the individual thermal wave phase profile (Fig. S1 in the supplementary material) were analyzed to determine the slope. The slopes were normalized by \sqrt{f} to obtain a quantity related to the inverse of diffusivity and plotted as a function of frequency in Fig. 2.^{8,45} The dashed and solid lines represent model fits of the experimental data by isotropic and anisotropic models of the ion track region, respectively. A better agreement of the anisotropic model with the experiment is direct evidence of anisotropic thermal conductivity in the patterned samples. Additional sensitivity analysis confirming that both conductivities can be extracted from these multifrequency measurements is presented in Fig. S2 in the supplementary material.

Measured thermal conductivities for in-plane and cross-plane directions are plotted in Fig. 3. It is important to note the trend in the evolution of the anisotropy in thermal transport. One typically expects anisotropy in thermal transport to decrease with the increase in disorder, as has been observed in previous studies.^{46,47} However, owing to the aligned nature of the defects, we observe that κ_r , despite being higher for the pristine sapphire, initially decreases much faster than κ_z with the ion dose but eventually becomes larger than κ_z for higher doses ($5 \times 10^{12} \text{ cm}^{-2}$) [Fig. 3(a)]. This intricate behavior where anisotropy switches direction two times can be attributed to directional phonon scattering with vertically aligned channels and phonon confinement effects. The observed slower in-plane conductivity reduction at the higher doses is likely due to saturation of ion-track density caused by damage recovery in the track overlapping regime.

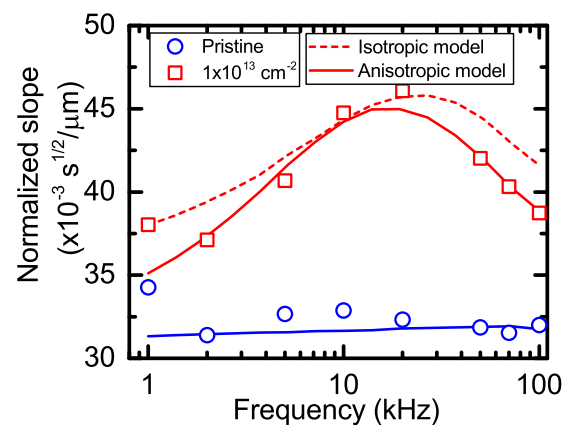


FIG. 2. Comparison of frequency dependent linear sections of phase profiles in patterned (red squares) and pristine (blue circles) sapphire. Analysis of measured phase profiles using isotropic (dashed line) and anisotropic (solid line) models reveal thermal conductivity anisotropy.

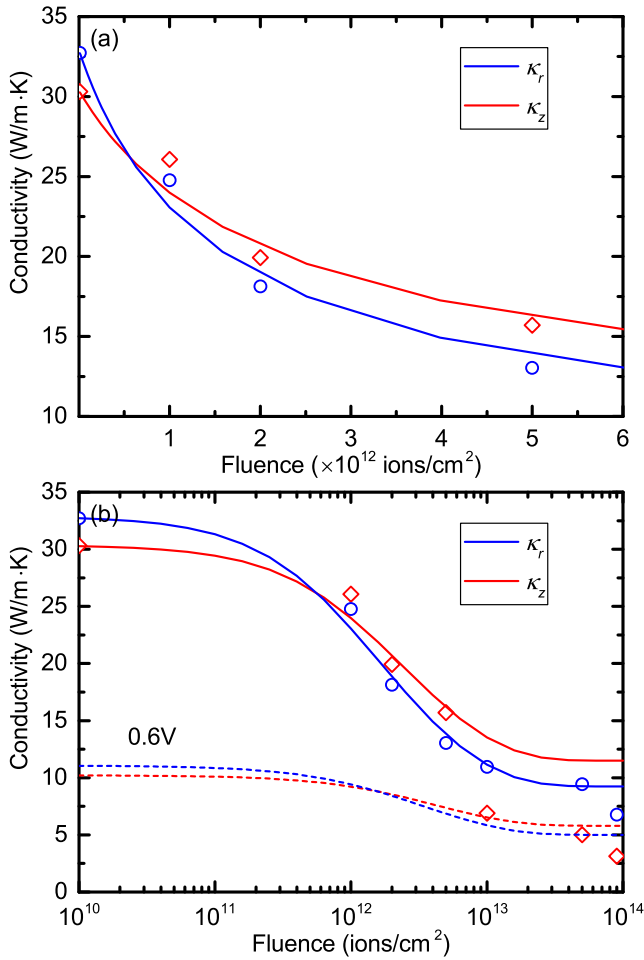


FIG. 3. (a) Cross-plane and in-plane thermal conductivity decay with SHI fluence in the isolated ion-track regime ($< 5 \times 10^{12}$ ions/cm²) using intrinsic velocities in sapphire. (b) Thermal conductivity model in cross-plane and in-plane directions with 40% reduction in cross-plane and in-plane velocities. Blue circles and red diamonds represent measured in-plane and cross-plane thermal conductivities, respectively. Solid lines represent the model that considers only ion track scattering, and dashed lines assume additional reduction in velocity caused by phonon confinement.

First, we consider low dose irradiations, corresponding to the isolated ion-track regime, where the region outside of the few nanometer diameter ion track core remains crystalline. The larger decrease in in-plane conductivity is attributed to the directional nature of phonon scattering with ion-tracks. This can be conveniently understood when one considers the specular boundary scattering event where the momentum of phonons parallel to the boundaries is preserved, while the perpendicular momentum is changed. This effect causes cross-plane propagating phonons to have a longer mean free path than in-plane ones and makes heat transfer parallel to ion tracks more efficient than that perpendicular to them. These observations provide a validation for the recent theoretical work that proposed that specular reflections lead to a larger reduction of conductivity in the direction perpendicular to the interface,

whereas conductivity parallel to the interfaces is impacted to a lesser extent.^{44,48} Moreover, in the isolated ion track regime, precise control of the ion track core boundary roughness can be used to tailor the specularly parameter and to further expand the understanding of nanoscale thermal transport.

At the higher dose, two competing effects are expected to play a role. First, when ion tracks overlap, the interface is likely to be more disordered. This results in diffuse scattering of phonons with ion tracks, thus effectively reducing the strength of directional scattering present due to specular reflection in the isolated track regime. The second effect, which is believed to be more pronounced, is attributed to the fact that, at high ion doses, the spacing between ion tracks is estimated to be on the order of 10 nm giving rise to phonon confinement effects. The phonon confinement induced change in phonon dispersion has been previously demonstrated in porous sapphire, where a correlation between thermal conductivity reduction and changes in the acoustic velocities was observed.¹⁵ A related computational work on the silicon based phononic crystal considered an aligned array of cylinders and thin films. In that study, it was demonstrated that there is a larger reduction in both acoustic velocity and conductivity parallel to the cylinder axis.^{4,15}

To validate the qualitative observations presented above, we use an analytical model that considers a single acoustic branch averaged over one longitudinal and two transverse branches with linear dispersion $\omega = v_k k$, where k is the phonon wavenumber, ω is its frequency, and v_k is its velocity along the direction of k .²⁴ An expression for anisotropic thermal conductivity that explicitly includes the contribution of phonons propagating in different directions and approximates the Brillouin zone by a sphere in the k -space is defined as

$$\kappa_i(r \text{ or } z) = \frac{3}{8\pi^3} \int_0^{k_D} k^2 dk \int_0^{2\pi} d\phi \int_0^\pi \frac{k_B x^2 e^x}{(e^x - 1)^2} v_i^2 \tau_{c,i} \sin \theta d\theta, \quad (2)$$

where $x = \frac{\hbar\omega}{k_B T}$, k_B is the Boltzmann constant, τ_c is the total phonon relaxation time, ω is the phonon frequency, \hbar is the reduced Planck's constant, and T is the absolute temperature. The integration limit k_D considering spherical approximation of the Brillouin zone is defined using $k_D^3 = 6\pi^2/\Omega_0$, where $\Omega_0 = 8.51 \times 10^{-30}$ m³ is the volume per atom. The phonon direction is defined by azimuthal θ and polar ϕ angles with respect to the z axis. v_i is the phonon velocity projection along the heat flux direction defined as $v_z = v(\theta)\cos\theta$ and $v_r = v(\theta)\sin\theta\cos\phi$, where $v(\theta)$ is the sound velocity obtained by solving the Christoffel equation and approximated by $v(\theta) = [v_c^2 \cos^2 \theta + v_a^2 \sin^2 \theta + v_m^2 \sin^2 2\theta]^{1/2}$ and the weak polar angle dependence is neglected. For sapphire, v_c , v_a , and v_m are estimated to be 7177, 7346, and 2145 m/s based on elastic constants.⁴⁹

Phonon relaxation time is a combination of anharmonic three-phonon (τ_U), defect (τ_D), and boundary (τ_B) scattering terms added using Matthiessen's rule. The three-phonon or Umklapp scattering process defines thermal resistance only due to crystal anharmonicity, and its phonon relaxation time is given as $\frac{1}{\tau_{U,i}} = \frac{2\gamma_i^2 k_B T \omega^2}{\rho v_{T,i}^2 \Omega_0 \omega_D}$, where γ is the Gruneisen anharmonicity parameter, $\rho = 3980$ kg/m³ is the density of sapphire, $v_{T,r} = 6630$ m/s and $v_{T,z} = 6120$ m/s, and $\omega_D = \nu k_D$ is the Debye frequency. $\gamma_r = 1.7$ and $\gamma_z = 1.6$ were obtained by fitting the calculated intrinsic conductivity to the experimental values.⁵⁰ The defect relaxation

time considers scattering by intrinsic impurities and is given by $\frac{1}{\tau_{D,i}}$ = $\frac{\Omega_0 \omega^4}{4\pi v_i^3} \Gamma$, where Γ is a defect cross section and estimated to be 0.061 for the undamaged sample.

For the phonon-track boundary scattering rate, τ_B , we use an expression previously considered for nanowires that accounts for specularity and is based on an average distance traveled by a phonon inside a cylinder,²⁴

$$\frac{1}{\tau_{B,i}} = \frac{1 - p_i}{1 + p_i} \frac{3\pi |\sin \theta|}{4} \frac{v_i}{D_a}, \quad (3)$$

where $p_i = \exp\left(-\frac{16\pi^2 \eta^2 \omega^2}{v_i^2}\right)$ is the specularity parameter defined by surface roughness η of the interface and D_a is the effective diameter of a cylindrical domain defined by nearest neighbor tracks. The direct impact model, $\alpha = \alpha_0(1 - e^{-\sigma\Phi})$,^{51,52} which is used to estimate damaged volume fraction, was employed to define the dose dependent domain size,

$$D_a^{-1} = D_0^{-1}(1 - e^{-\sigma\Phi}), \quad (4)$$

where α is a disorder parameter, $\sigma = 12 \times 10^{-14} \text{ cm}^{221}$ is the damage cross section, Φ is the ion fluence, and $D_0 = 3.8 \text{ nm}$ is the effective hydraulic diameter of the channel defined by ion tracks.

This model was used to calculate the thermal conductivity at different fluences and was found to provide a reasonable agreement for the isolated ion-track regime (or low fluence, $\leq 5 \times 10^{12} / \text{cm}^2$) for both cross-plane and in-plane values of thermal conductivities when surface roughness $\eta = 0.012 \text{ nm}$ was considered [Fig. 3(a)]. However, this model is unable to capture the behavior at high fluences, especially for κ_z . Model calculation in the diffuse limit $p = 0$ for cross-plane conductivity agrees with the experiment, but it underestimates the measured in-plane conductivity (not shown). While the current model captures the trends of anisotropic conductivity evolution at a low dose, we suspect it is not to be relied upon for accurate analysis as the current fit of surface roughness is unphysical and not supported by TEM analysis. We attribute this discrepancy to the oversimplified treatment of phonon dispersion and phonon-track boundary scattering. More detailed analysis considering branch specific analysis, accurate representation of anharmonic effects, and phonon-track scattering is expected to provide more realistic results. Most notably, the current model fails to predict a significant reduction in the cross-plane conductivity in the perfectly specular limit, $p = 1$.⁴⁸

We were able to reproduce cross-plane conductivity in the high frequency regime, when a (~40%) reduction of phonon velocity in the cross-plane direction (Fig. 3) was considered supporting the phonon confinement scenario in the high fluence regime.^{4,15} Our observations are consistent with a previous study by Kargar *et al.*¹⁵ which reported a ~10% reduction in cross-plane velocity for a sample with 25-nm-diameter nanopores.

In conclusion, the SHI irradiation of sapphire is an attractive avenue to tailor its anisotropic thermal conductivity. The higher rate of decay for κ_r in the low fluence regime is attributed to the partially specular reflection of phonons from ion tracks, thereby affecting in-plane transport more than cross-plane transport. In contrast, in the high fluence regime, larger reduction of κ_z is attributed to the phonon confinement effect causing modification in phonon dispersion due to the high density of ion tracks. Therefore, ion

track patterning offers opportunities for tailoring anisotropic thermal transport properties of insulating materials and enables studies of nanoscale thermal transport.

The [supplementary material](#) provides the example of thermoreflectance profiles and sensitivity analysis.

V.S.C and A.A. thank Kevin Agarwal for help in MTR measurements. V.S.C. and M.K. acknowledge funding support of the Center for Thermal Energy Transport under Irradiation (TETI), an Energy Frontier Research Center by the U.S. Department of Energy, Office of Science, Office of Basic Energy Sciences. A.A. and Z.U. acknowledge funding support of Grant No. AP05130446 and state-targeted Program No. BR05236454 by Kazakhstan Ministry of Education and Science, Grant No. AP06851392 by Kazakhstan Ministry of Industry and Infrastructural Development, and FDCR Grant No. 110119FD4501 by Nazarbayev University.

REFERENCES

- H. J. Goldsmid, *J. Electron. Mater.* **40**(5), 1254–1259 (2011).
- D. G. Cahill, W. K. Ford, K. E. Goodson, G. D. Mahan, A. Majumdar, H. J. Maris, R. Merlin, and S. R. Phillpot, *J. Appl. Phys.* **93**(2), 793–818 (2002).
- D. G. Cahill, P. V. Braun, G. Chen, D. R. Clarke, S. Fan, K. E. Goodson, P. Keblinski, W. P. King, G. D. Mahan, A. Majumdar, H. J. Maris, S. R. Phillpot, E. Pop, and L. Shi, *Appl. Phys. Rev.* **1**(1), 011305 (2014).
- Z. Wei, G. Wehmeyer, C. Dames, and Y. Chen, *Nanoscale* **8**(37), 16612–16620 (2016).
- D. J. Renteria, L. D. Nika, and A. A. Balandin, *Appl. Sci.* **4**(4), 525–547 (2014).
- S. Ghosh, I. Calizo, D. Teweldebrhan, E. P. Pokatilov, D. L. Nika, A. A. Balandin, W. Bao, F. Miao, and C. N. Lau, *Appl. Phys. Lett.* **92**(15), 151911 (2008).
- J. Zhang, H. J. Liu, L. Cheng, J. Wei, J. H. Liang, D. D. Fan, P. H. Jiang, and J. Shi, *Sci. Rep.* **7**(1), 4623 (2017).
- Y. Wang, D. H. Hurley, E. P. Luther, M. F. Beaux, D. R. Vodnik, R. J. Peterson, B. L. Bennett, I. O. Usov, P. Yuan, X. Wang, and M. Khafizov, *Carbon* **129**, 476–485 (2018).
- M. Zeraati, S. M. Vaez Allaei, I. Abdolhosseini Sarsari, M. Pourfath, and D. Donadio, *Phys. Rev. B* **93**(8), 085424 (2016).
- C. Yuan, J. Li, L. Lindsay, D. Cherns, J. W. Pomeroy, S. Liu, J. H. Edgar, and M. Kuball, *Commun. Phys.* **2**(1), 43 (2019).
- Z. Aksamija and I. Knezevic, *Phys. Rev. B* **82**(4), 045319 (2010).
- V. Poborchii, N. Uchida, Y. Miyazaki, T. Tada, P. I. Geshev, Z. N. Utegulov, and A. Volkov, *Int. J. Heat Mass Transfer* **123**, 137–142 (2018).
- G. Zhu, J. Liu, Q. Zheng, R. Zhang, D. Li, D. Banerjee, and D. G. Cahill, *Nat. Commun.* **7**, 13211 (2016).
- B. Sun, G. Haunschild, C. Polanco, J. Ju, L. Lindsay, G. Koblmueller, and Y. K. Koh, *Nat. Mater.* **18**(2), 136–140 (2019).
- F. Kargar, S. Ramirez, B. Debnath, H. Malekpour, R. K. Lake, and A. A. Balandin, *Appl. Phys. Lett.* **107**(17), 171904 (2015).
- J. H. O'Connell, R. A. Rymzhanov, V. A. Skuratov, A. E. Volkov, and N. S. Kirilkin, *Nucl. Instrum. Methods Phys. Res., Sect. B* **374**, 97–101 (2016).
- P. N. M. Ngoepe, W. E. Meyer, F. D. Auret, E. Omotoso, T. T. Hlatshwayo, V. A. Skuratov, and M. Diale, *Nucl. Instrum. Methods Phys. Res., Sect. B* **409**, 69–71 (2017).
- W. J. Weber, E. Zarkadoula, O. H. Pakarinen, R. Sachan, M. F. Chisholm, P. Liu, H. Xue, K. Jin, and Y. Zhang, *Sci. Rep.* **5**, 7726 (2015).
- N. Sellami, M. L. Crespillo, Y. Zhang, and W. J. Weber, *Mater. Res. Lett.* **6**(6), 339–344 (2018).
- A. Kabir, A. Meftah, J. P. Stoquert, M. Toulemonde, and I. Monnet, *Nucl. Instrum. Methods Phys. Res., Sect. B* **266**(12), 2976–2980 (2008).
- A. Kabir, A. Meftah, J. P. Stoquert, M. Toulemonde, I. Monnet, and M. Izerrouken, *Nucl. Instrum. Methods Phys. Res., Sect. B* **268**(19), 3195–3198 (2010).

- ²²E. R. Dobrovinskaya, L. A. Lytvynov, and V. Pishchik, *Sapphire: Material, Manufacturing, Applications* (Springer, Boston, MA, 2009), pp. 55–176.
- ²³P. E. Hopkins, T. Beechem, J. C. Duda, K. Hattar, J. F. Ihlefeld, M. A. Rodriguez, and E. S. Piekos, *Phys. Rev. B* **84**(12), 125408 (2011).
- ²⁴A. J. H. McGaughey, E. S. Landry, D. P. Sellan, and C. H. Amon, *Appl. Phys. Lett.* **99**(13), 131904 (2011).
- ²⁵M. Upadhyaya, S. N. Khatami, and Z. Aksamija, *J. Mater. Res.* **30**(17), 2649–2662 (2015).
- ²⁶Z. Wei, Y. Chen, and C. Dames, *Appl. Phys. Lett.* **102**(1), 011901 (2013).
- ²⁷C. Huang, X. Zhao, K. Regner, and R. Yang, *Physica E* **97**, 277–281 (2018).
- ²⁸A. Malhotra and M. Maldovan, *J. Appl. Phys.* **120**(20), 204305 (2016).
- ²⁹A. Malhotra and M. Maldovan, *Sci. Rep.* **6**, 25818 (2016).
- ³⁰J. F. Ziegler, M. D. Ziegler, and J. P. Biersack, *Nucl. Instrum. Methods Phys. Res., Sect. B* **268**(11), 1818–1823 (2010).
- ³¹P. V. Vladimirov, D. Lizunov, Y. A. I. Ryazanov, and A. Möslang, *J. Nucl. Mater.* **253**(1), 104–112 (1998).
- ³²R. A. Rymzhanov, N. Medvedev, A. E. Volkov, J. H. O’Connell, and V. A. Skuratov, *Nucl. Instrum. Methods Phys. Res., Sect. B* **435**, 121–125 (2018).
- ³³V. A. Skuratov, J. O’Connell, N. S. Kirilkin, and J. Neethling, *Nucl. Instrum. Methods Phys. Res., Sect. B* **326**, 223–227 (2014).
- ³⁴R. A. Rymzhanov, N. Medvedev, J. H. O’Connell, A. J. van Vuuren, V. A. Skuratov, and A. E. Volkov, *Sci. Rep.* **9**(1), 3837 (2019).
- ³⁵J. Pakarinen, M. Khafizov, L. He, C. Wetteland, J. Gan, A. T. Nelson, D. H. Hurley, A. El-Azab, and T. R. Allen, *J. Nucl. Mater.* **454**(1–3), 283–289 (2014).
- ³⁶M. Khafizov, V. Chauhan, Y. Wang, F. Riyad, N. Hang, and D. H. Hurley, *J. Mater. Res.* **32**(1), 204–216 (2016).
- ³⁷D. H. Hurley, R. S. Schley, M. Khafizov, and B. L. Wendt, *Rev. Sci. Instrum.* **86**(12), 123901 (2015).
- ³⁸A. J. Schmidt, R. Cheaito, and M. Chiesa, *Rev. Sci. Instrum.* **80**(9), 094901 (2009).
- ³⁹D. G. Cahill, *Rev. Sci. Instrum.* **75**(12), 5119–5122 (2004).
- ⁴⁰M. Khafizov and D. H. Hurley, *J. Appl. Phys.* **110**(8), 083525 (2011).
- ⁴¹M. F. Riyad, V. S. Chauhan, and M. Khafizov, *J. Nucl. Mater.* **509**, 134–144 (2018).
- ⁴²D. Cahill, S. K. Watson, and R. Pohl, *Phys. Rev. B* **46**, 6131 (1992).
- ⁴³A. Cappella, J.-L. Battaglia, V. Schick, A. Kusiak, A. Lamperti, C. Wiemer, and B. Hay, *Adv. Eng. Mater.* **15**(11), 1046–1050 (2013).
- ⁴⁴A. Abdullaev, V. S. Chauhan, B. Muminov, J. O’Connell, V. A. Skuratov, M. Khafizov, and Z. N. Utegulov, “Thermal transport across nanoscale damage profile in sapphire irradiated by swift heavy ions,” *J. Appl. Phys.* (to be published).
- ⁴⁵M. Khafizov, J. Pakarinen, L. He, and D. H. Hurley, *J. Am. Ceram. Soc.* **102**(12), 7533–7542 (2019).
- ⁴⁶J. D. Renteria, S. Ramirez, H. Malekpour, B. Alonso, A. Centeno, A. Zurutuza, A. I. Cocemasov, D. L. Nika, and A. A. Balandin, *Adv. Funct. Mater.* **25**(29), 4664–4672 (2015).
- ⁴⁷M. N. Luckyanova, J. A. Johnson, A. A. Maznev, J. Garg, A. Jandl, M. T. Bulsara, E. A. Fitzgerald, K. A. Nelson, and G. Chen, *Nano Lett.* **13**(9), 3973–3977 (2013).
- ⁴⁸M. Maldovan, *J. Appl. Phys.* **125**(22), 224301 (2019).
- ⁴⁹W. G. Mayer and E. A. Hiedemann, *Acta Crystallogr.* **14**(3), 323 (1961).
- ⁵⁰G. H. Watson, W. B. Daniels, and C. S. Wang, *J. Appl. Phys.* **52**(2), 956–958 (1981).
- ⁵¹B. Canut, A. Benyagoub, G. Marest, A. Meftah, N. Moncoffre, S. M. M. Ramos, F. Studer, P. Thevenard, and M. Toulemonde, *Phys. Rev. B* **51**(18), 12194–12201 (1995).
- ⁵²W. J. Weber, *Nucl. Instrum. Methods Phys. Res., Sect. B* **166-167**, 98–106 (2000).